



HAL
open science

An easy synthesis of small, stable and water-compatible superparamagnetic protein-specific molecularly imprinted nanoparticles

Nébéwia Griffete, Laurent Michot, Carlo Gonzato

► To cite this version:

Nébéwia Griffete, Laurent Michot, Carlo Gonzato. An easy synthesis of small, stable and water-compatible superparamagnetic protein-specific molecularly imprinted nanoparticles. *Polymer*, 2022, 239, pp.124446. 10.1016/j.polymer.2021.124446 . hal-03765788

HAL Id: hal-03765788

<https://hal.sorbonne-universite.fr/hal-03765788>

Submitted on 31 Aug 2022

HAL is a multi-disciplinary open access archive for the deposit and dissemination of scientific research documents, whether they are published or not. The documents may come from teaching and research institutions in France or abroad, or from public or private research centers.

L'archive ouverte pluridisciplinaire **HAL**, est destinée au dépôt et à la diffusion de documents scientifiques de niveau recherche, publiés ou non, émanant des établissements d'enseignement et de recherche français ou étrangers, des laboratoires publics ou privés.

An easy synthesis of small, stable and water-compatible superparamagnetic protein-specific molecularly imprinted nanoparticles

Nébéwia Griffete^{1,*}, Laurent Michot¹ and Carlo Gonzato^{2,*}

¹ Dr. L. Michot and Dr. N. Griffete

Sorbonne Université, CNRS, PPhysico-chimie des Electrolytes et Nanosystèmes Interfaciaux, PHENIX
4 place jussieu, 75005 Paris, France; nebewia.griffete@sorbonne-universite.fr

² Université de Technologie de Compiègne, CNRS Laboratory for Enzyme and Cell Engineering UMR 7025,
Rue du Docteur Schweitzer, 60203, Compiègne, France

* Correspondance: nebewia.griffete@sorbonne-universite.fr and carlo.gonzato@utc.fr

Abstract: We report the synthesis of small (below 100 nm), stable and water-compatible superparamagnetic molecularly imprinted nanocomposites using water-soluble, dithiocarbamate-based photoiniferters. These agents were adsorbed directly on the surface of maghemite nanoparticles and allowed the synthesis of thin layers of molecularly imprinted polymer able to specifically and selectively bind green fluorescent protein as a model protein. To the best of our knowledge, this is the first time that water soluble photoiniferters have been used to prepare this kind of imprinted materials.

Keywords: magnetic nanoparticles, molecularly imprinted polymer, surface modification, protein

1. Introduction

Molecularly imprinted polymers (MIPs) are cross-linked polymer networks carrying recognition sites specific and selective for a target molecule which is introduced during their “templated” synthesis. Over the last few years, MIPs have become widely used for nanomedicine, (e.g.¹) thanks to their remarkable recognition properties as well as to the synthetic efforts made to render them small, stable and biocompatible, and thus, suitable for *in vivo* applications. Piletsky and co-workers developed for instance molecularly imprinted nanoparticles (nanoMIPs) against Epidermal Growth Factor Receptor (EGFR) able to specifically recognize a native protein and selectively deliver a drug payload to the corresponding cell target². The same group also developed MIPs against an extracellular epitope of a biomarker, which allowed the *in vitro* and *in vivo* detection of senescent cells³. Cecchini et al. also reported on the use of MIPs to specifically target cells in zebra fish embryos⁴, while Koide et al. could make MIPs capable of *in vivo* inhibiting the action of the human endothelial growth factor⁵.

Conversely to the well-established imprinting of small molecules, the imprinting of proteins is still very challenging⁶: such molecules are indeed big, their structure is rather flexible and they are very sensitive to their local environment, which means that imprinting must be carried out in a medium as favorable as possible to the protein structure (ie. water or aqueous buffers rather than organic solvents). This restriction limits in turn the choice of monomers, crosslinking agents and polymerisation initiators, which have to be water-soluble.

Superparamagnetic iron oxide nanoparticles (SPIONs) have as well been the subject of intensive research over the past few decades thanks to their low toxicity and remarkable magnetic properties, which allow for instance their use as contrast agent⁷. Exceptional hyperthermia properties have allowed SPIONs to be used, for instance, for cancer treatment or drug release^{8,9,10}. Combining SPIONs with MIPs has led to hybrid

41 materials with interesting biomedical applications, including targeting, imaging and even treatment
42 (hyperthermia). Griffete et al. developed for instance magnetic MIP able to release a cancer cells drug upon
43 local heating induced by an alternating magnetic field^{11,12,13}. On the other hand, a magnetif field can also be
44 used to guide magnetic materials toward a selected organ or a tumor, without necessarily using a MIP to
45 discriminate the target. In a recent study, Asadi and coworkers described, for instance, the sythesis of multi
46 core-shell nanocarriers loaded with 5-fluorouracil, a anticancer drug with fast degradation rates¹⁴.

47 However, for their *in vivo* use, superparamagnetic MIPs have to be small (i.e. below 100 nm), stable and
48 water-compatible. A common strategy to fit these requirements consists in coating SPIONs with a silica layer
49 *via* sol-gel chemistry, followed by the grafting of a polymer (functional) layer¹⁵. However, this approach
50 increases the size of magnetic NPs, due to the thickness of the silica layer which sits on top of the usual
51 aggregation of NPs often observed during their coating. Thus, to keep particles' size as small as possible, a
52 direct coating of SPIONs with a functional layer would be preferred. Surprisingly, only few works have
53 reported on the synthesis of hybrid magnetic MIPs by directly growing an imprinted shell on the surface of
54 SPIONs¹⁶. Indeed, a great majority of hybrid magnetic MIPs is obtained using silica-coated SPIONs. This
55 approach is easier and allows protecting the magnetic core while providing the NPs' surface with reactive
56 functional groups, such as amines (e.g. APTES) or polymerizable double bonds (e.g. MPTMS), for the
57 subsequent polymer grafting¹⁷. The resulting composites are then often dispersed in an organic solvent where
58 an imprinted layer is obtained either by free-radical of more frequently reversible deactivation radical
59 polymerisation (RDRP). This latter approach has emerged as an efficient way of tuning both the thickness of
60 the imprinted layer, as well as its surface chemistry due to the possibility of chain extension *via* consecutive
61 blocks¹⁸. Among the different RDRP techniques, reversible addition-fragmentation chain-transfer (RAFT) and
62 stable free-radical polymerization (SFRP) in its iniferter form are the most widely used by the imprinting
63 community¹⁹.

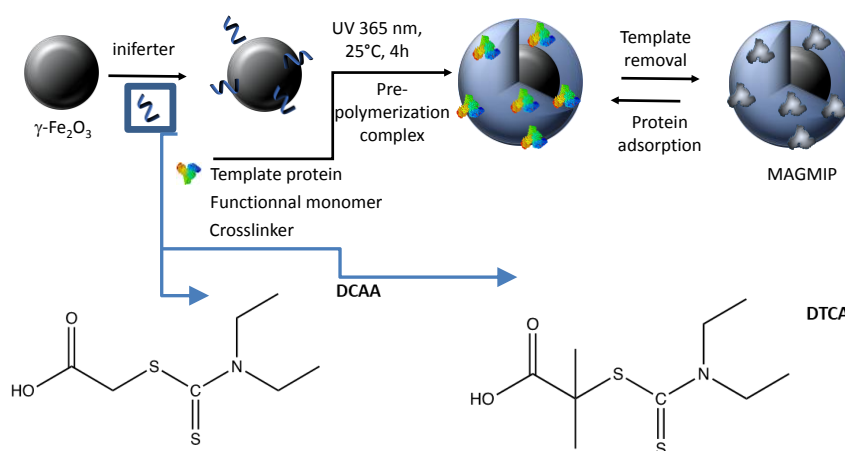
64 Introduced by Otsu in 1982, iniferters²⁰ (standing for *initiator*, *transfer* agent and *terminator*) are chemical
65 species undergoing reversible bond cleavage to produce an active, propagating radical responsible for
66 polymer growth, and a dormant species unable to propagate but capable of reversible coupling to regenerate
67 the iniferter species. In addition to supporting a reversible dissociation, iniferters are also capable of
68 degenerative transfer, so that their ability in controlling a radical polymerisation results from a balance of
69 reversible dissociation/coupling and chain transfer (scheme S1).

70 Conversely to the case of organic solvents, direct modification and polymerization of SPIONs in water, on the
71 other hand, is less obvious, due to the limited choice of water-soluble initiators capable of both SPIONs'
72 stabilization and RDRP. In the case of photoiniferters, the commonly used, hydrophobic benzyl
73 N,N-diethyldithiocarbamate (BDC) would indeed simply not be soluble.

74 To overcome this problem, we thus report herein, the use of two water-soluble photoiniferters based on
75 dithiocarbamates (Scheme 1) which allow the synthesis of small, stable and water-soluble superparamagnetic
76 molecularly imprinted nanoparticles able to specifically and selectively recognize green fluorescent protein
77 (GFP) as model protein. Such water soluble photoiniferters simultaneously behave as SPIONs stabilizers and
78 initiators for the polymerization of thin layers of MIP under UV irradiation at 365nm and in buffer solution.
79 To the best of our knowledge, this is the first time that water soluble photoiniferters have been used to directly coat
80 SPIONs with an imprinted later in aqueous media.

81

82



Scheme 1. Synthetic process used to obtain small and stable Fe₂O₃@MIP nanoparticles. DCAA stands for 2-(N,N-diethyldithiocarbamyl)acetic acid whereas DTCA for 2-(N,N-diethyldithiocarbamyl)isobutyric acid.

2. Experimental section

2.1. Materials

Sodium diethyldithiocarbamate trihydrate (NaDTC), 2-bromo-2-methylpropionic acid (2-BrMPA), sodium chloroacetate, 6% hydrochloric acid, Ovalbumin (OVA, molecular weight (Mw): 42.7 kDa and isoelectric point (pI): 4.7), bovine serum albumin (BSA, Mw: 66.5 kDa and pI: 4.9), acrylamide (AM), N,N-methylene-bis-acrylamide (MBAM), and 4-(2-hydroxyethyl)-1-piperazine-ethanesulfonic acid (HEPES) were from Sigma (Saint-Quentin Fallavier, France). Iron (II) chloride tetrahydrate (FeCl₂·4H₂O), iron (III) chloride hexahydrate (FeCl₃·6H₂O), methanol Acetone (rectapur), diethyl ether, ferric nitrate and concentrated hydrogen chloride (normapur) were from VWR Chemicals (Strasbourg, France). Acetic acid and ammonia at 22.5% were from Carlo Erba. The green fluorescent protein (GFP, Mw: 32.7 kDa and pI: 5.7) was kindly donated by the Dahan group of the Curie Research Institute. Deionized water (resistivity ≥ 18.2 M Ω cm⁻¹) was obtained using a Milli-Q plus unit (Millipore, Molsheim, France). DMSO-d₆ and CDCl₃ were from Eurisotop (Saint-Aubin, France).

2.2. Instrumentation

Transmission Electron Microscopy (TEM). Nanoparticles were observed using a Jeol-100 CX TEM. A droplet of diluted nanoparticles suspension in water was deposited on a carbon coated copper grid and the excess was drained using filter paper. Size analysis was achieved on TEM images using ImageJ software.

Dynamic light scattering (DLS). Hydrodynamic diameter (dh) measurements were recorded using a Malvern Instruments Nanosizer operating at 633 nm at 25 C.

Fourier Transform Infra-Red (FT-IR.) FT-IR spectra were recorded on a Bruker Tensor 27 spectrometer on pressed KBr pellets. Spectra were obtained at regular time intervals in the MIR region of 4000 – 400 cm⁻¹ at a resolution of 4 cm⁻¹ and analyzed using OPUS software.

Ultraviolet-visible spectrophotometry (UV-vis). Absorption spectra were recorded on a Cary 60 UV-vis (Agilent Technologies) from 230 to 500 nm, with a 1 nm resolution.

NMR experiments: ¹H NMR spectra in DMSO-d₆ and CDCl₃ were recorded on a 400 MHz Bruker spectrometer at 25 °C.

Iron Titration. The total iron concentration (M) was determined by atomic absorption spectroscopy (AAS) with a Perkin-Elmer Analyst 100 apparatus after degradation of $\gamma\text{-Fe}_2\text{O}_3$ NPs in boiling HCl (35%).

SAXS. SAXS measurements were performed at the Swing SAXS beamline of the SOLEIL synchrotron radiation facility at Saint-Aubin, France. The X-ray energy was 12.0 keV, corresponding to the wavelength $\lambda=0.1033$ nm, and a q-range between 10^{-1} and 1 nm $^{-1}$. Two samples-to-detector distances of 6.226 m and 0.57 m were used and the beam-size at the sample was 375×75 m 2 . Typical exposure times were around 500ms and the scattering patterns were recorded with a Eiger-4 M detector. The 2D images obtained were treated by classical data reduction procedures and azimuthal averaging of the SAXS patterns provided plots of the scattered intensity versus scattering vector modulus, $I(q)$. Samples were filled into cylindrical Lindemann glass capillaries of 1.0 ± 0.1 mm diameter and sealed by flame. An empty capillary and a water-filled one were also measured, which allowed subtracting the signal from both the container and the solvent.

2.3. Synthesis of γ -Fe $_2$ O $_3$

The synthesis presented here leads to a large amount of Fe $_2$ O $_3$ nanoparticles, but only a very small quantity of this synthesis will be used further. Briefly, 0.905 mol of ferrous chloride and 1.59 mol of ferric chloride were dissolved in 6% hydrochloric acid. 1 L of ammonia at 22.5% was added to the medium, under vigorous magnetic stirring at room temperature. Reaction was allowed to continue for 30 minutes. Then, the as-obtained magnetite was oxidized using 0.80 mol of ferric nitrate. The suspension was heated at 100°C under magnetic stirring for 30 minutes in order to speed up the oxidation of the particles. Maghemite nanoparticles were then washed three times with acetone and two times with diethyl ether, before being dispersed in water.

2.4. Synthesis of the photoiniferter 2-(N,N-diethyldithiocarbamyl)isobutyric acid DTCA

The synthesis of DTCA was according to Ishizu et al.²¹ with some modifications. Briefly, in a 20 mL glass vial sealed with a screw cap, NaDTC (8 mmol) and acetone (5 mL) were mixed together and magnetically stirred at room temperature. In a separate vial, 2-BrMPA (8 mmol) was dissolved in acetone (5 mL) and added dropwise to the former dispersion under vigorous stirring. The resulting mixture was then transferred in an oil bath and magnetically stirred at 40 °C for 16 hours, shielded from light with an Al foil. The resulting yellowish dispersion was then filtered to remove NaBr and concentrated under reduced pressure before being precipitated into an excess (30 mL) of acid solution at pH 1.5 (HCl) to afford DTCA as a white solid. Upon filtration and drying at 50 °C, DTCA was obtained in 40 % yield. 1 H-NMR (DMSO- d_6): 1.15-1.23 ppm (m, 6H), 1.59, (s, 6H), 3.66-3.88 (2 q, 4H).

2.5. Synthesis of the photoiniferter 2-(N,N-diethyldithiocarbamyl)acetic acid (DCAA)

The synthesis of DTCA was according to Sunayama et al.²² with some modifications. Briefly, in a 50 mL glass flask sealed with a cap, NaDTC (8 mmol) was mixed in water (10 mL) under magnetic stirring. Upon complete dissolution, sodium chloroacetate (8 mmol) in water (10 mL) was added dropwise and the resulting mixture was allowed to stir at room temperature for 2 days shielded from light with an Al foil. The reaction flask was cooled on ice and the pH of the solution was adjusted to 1.5 with conc. HCl. DCAA appeared as a white precipitate which was collected by filtration, washed with some water and dried overnight at 50 °C to afford a white solid in 90 % yield. 1 H-NMR (CDCl $_3$): 1.28-1.36 ppm (m, 6H), 3.76-4.06 (2 q, 4H), 4.21 (s, 2H).

2.6. Surface modification of the magnetic nanoparticles with DCAA and DTCA

Nanoparticles surface was functionalized using either DCAA or DTCA synthesized as previously described, later called only "initiator". 10 mg of the initiator were dissolved in 30 mL of distilled water, followed by the addition of 2 mL of an aqueous dispersion of magnetic nanoparticles (dry extract: 740 mg). Functionalization reaction was allowed to proceed at room temperature under orbital stirring at 320 rpm for 24 h, in plastic tubes covered with aluminium foils

to preserve the light-sensitive initiators. Then, functionalized nanoparticles were dialyzed using distilled water. Dialysis also occurred in a beaker protected from direct light and UV-irradiation.

2.7. MIP and NIP synthesis

0.33 μmol of GFP and 360 μmol of acrylamide were dissolved in 8 mL of HEPES, pH = 8, 200 mM. We then added 65 μmol ($R = 5.54$) of the cross-linking agent, N,N-methylene-bis-acrylamide. The pre-polymerization complex was then allowed to form under orbital stirring at 240 rpm for two hours. Afterwards, 215 μL of aqueous dispersion of iniferter-coated SPIONS (corresponding to 5 mg of particles), were added to the reaction medium. The mixture was nitrogen purged for 20 minutes and the polymerisation was allowed to proceed under orbital stirring at 240 rpm and UV- irradiation at 365 nm (Lamp UVA - UVC 13728- Pierron, 7 uW/cm^2 , with a distance of 10cm between the flask and the source) for 4 hours. The final product was washed thoroughly with deionised water using a dialysis membrane, in order to remove unreacted monomers and unbound protein. Polymer coated SPIONs were further washed with a 9/1 methanol/acetic acid mixture and distilled water in order to remove the template protein. Non-imprinted polymers were synthesized using the same protocol except that the protein was missing.

2.8. Protein adsorption experiments

The adsorption capacities (Q) of the different magnetic imprinted polymers and the magnetic non-imprinted polymer nano-objects were determined as follows: 5 mg of the materials were dispersed in 3 mL of water containing different concentrations of protein. The resulting mixtures were incubated at room temperature for 24 hours. Particles were collected by an external magnetic field and supernatants were analysed. The adsorption capacity was determined as follows:

$$Q = \frac{(C_i - C_f)V}{m}$$

where C_i (mg/mL) and C_f (mg/mL) are respectively the initial and final concentrations of the protein samples, determined using UV-Vis spectrophotometry, V (mL) is the volume of the protein solution and m (mg) is the mass of the nano-objects initially dispersed.

2.9. Selectivity determination and competitive binding assay

Ovalbumin (OVA) and bovin serum albumin (BSA) were chosen to investigate the selectivity of the MIP toward GFP. Experiments were carried out as described above to determine the adsorption capacity of the imprinted polymers toward these proteins.

3. Results and discussion

Figure 1 shows TEM images of the maghemite-based SPIONs ($\gamma\text{-Fe}_2\text{O}_3$) that we obtained by co-precipitation as reported by Massart¹ et al.. They feature a standard average size of 11 nm. We then functionalized their surface with an iniferter agent (either 2-(N,N-diethyldithiocarbamyl)acetic acid DCAA²³ or 2-(N,N-diethyldithiocarbamyl)isobutyric acid DTCA²¹) and we polymerised the resulting dispersions using GFP as model protein in order to obtain a MIP layer (see the experimental section). Both dithiocarbamates behave as photoiniferters thanks to the reversible dissociation of the C-S bond²³ upon irradiation at 365 nm (Figure S1) which allows tuning the thickness of the polymer layer. TEM analysis on Fe_2O_3 @DTCA and Fe_2O_3 @DCAA and later Fe_2O_3 @DTCA-MIP and Fe_2O_3 @DCAA-MIP revealed a slight size increase upon photoiniferter-coating, and a much bigger increase upon polymerisation. Aggregation upon DCAA or DTCA adsorption is not surprising, but the relatively small sizes (below 40 nm) of such composited leave enough "room" to the MIP layer. Interestingly, upon

polymerization, magnetic MIPs feature an average size of respectively 40nm (Figure 1A) and 80 nm, (Figure 1B) both suitable for biomedical applications²⁴. Fe₂O₃@DTCA-MIP showed a thinner layer (2 nm) compared to Fe₂O₃@DCAA-MIP (5 nm), which possibly relates to a better polymerization control achieved with DTCA and associated to an easier dissociation compared to DCAA. To assess the stability of the particles, we measured by DLS their hydrodynamic diameter 6 months after their synthesis. The thus determined sizes ($D_h=68.9$ nm for Fe₂O₃@DTCA@MIP and $D_h=129.2$ nm for Fe₂O₃@DCAA@MIP) are very similar to the initial ones, which shows that the particles we synthesized do not significantly evolve with time.

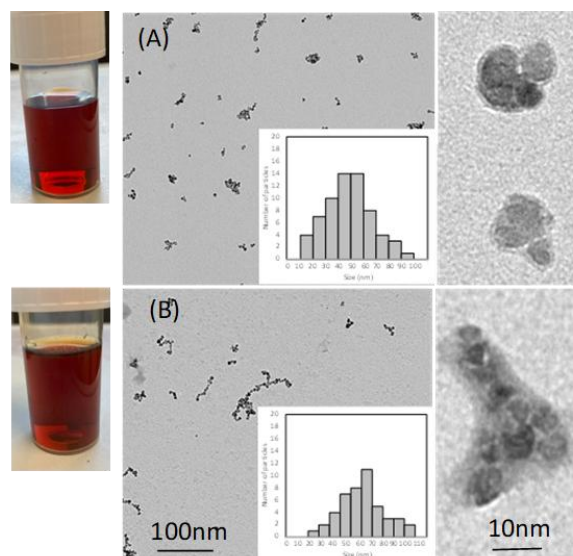


Figure 1. Representative TEM images of Fe₂O₃@MIP nanocomposites obtained using A) DTCA and B) DCAA as photoiniferter agents.

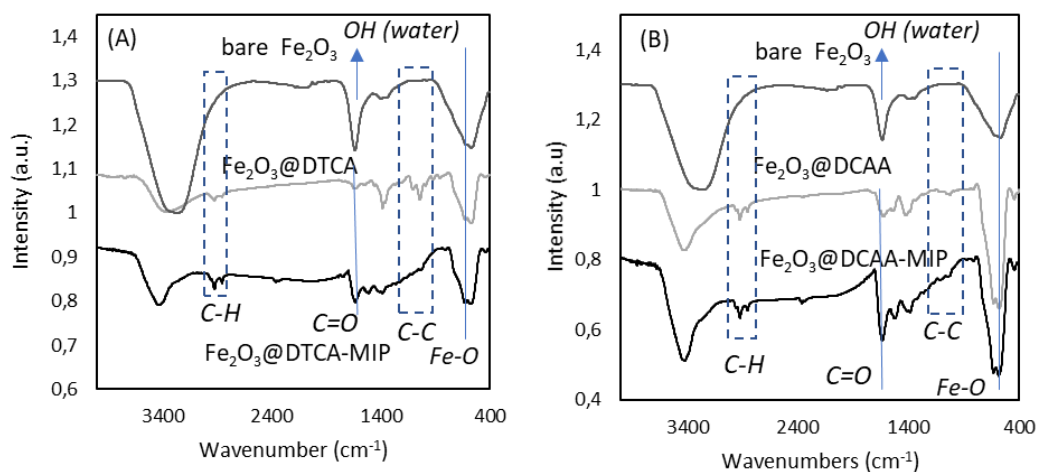
The sizes measured by TEM agree well with those obtained by DLS (Table 1).

Sample	Diameter in TEM (nm)	Hydrodynamic diameter in DLS (nm)	PDI (DLS)
γ -Fe ₂ O ₃	10	18	0.174
Fe ₂ O ₃ @DTCA	12	28	0.255
Fe ₂ O ₃ @DTCA@MIP	40	50	0.324
Fe ₂ O ₃ @DCCA	14	31	0.352
Fe ₂ O ₃ @DCCA@MIP	80	120	0.261

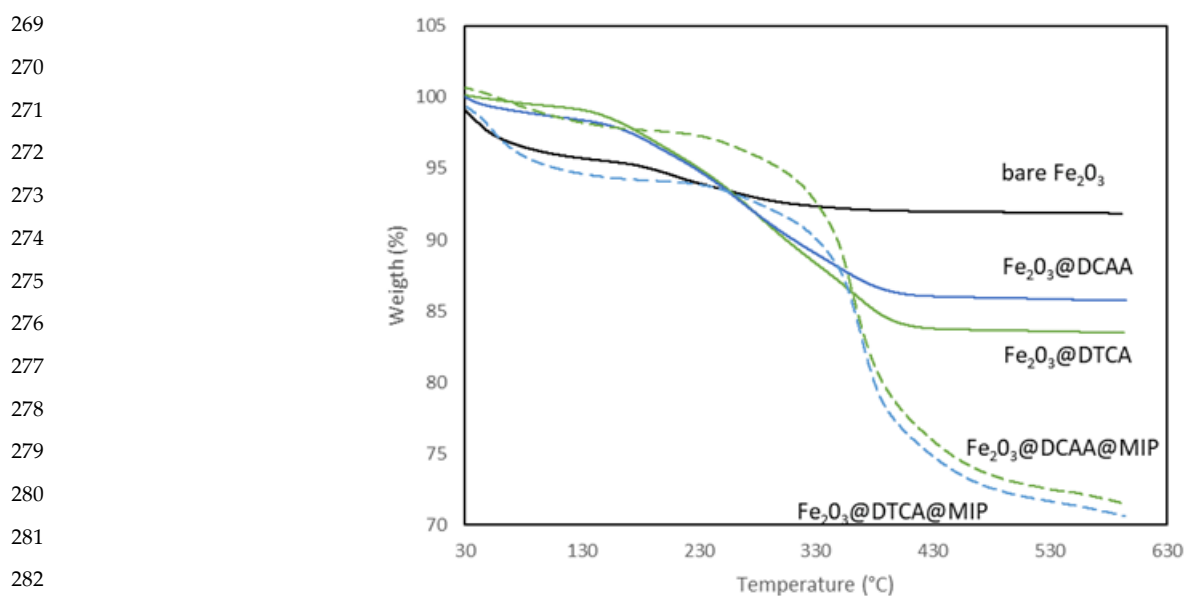
Table 1. Diameter and Hydrodynamic diameter of the particles measured in TEM and DLS with its polydispersity index.

As expected, the polymer coating did not influence the superparamagnetic properties, as shown by the absence of hysteresis in figure S3. To assess the effectiveness of the different synthetic steps, Fourier transform infrared (FT-IR) on bare, photoiniferter-functionalized and MIP-coated SPIONs were recorded (Figure 2). Iron oxide nanoparticles present characteristic peaks at 628 cm⁻¹ and 580 cm⁻¹ corresponding to the Fe-O vibration. The synthesized maghemite NPs bear residual -OH groups on their surface (which becomes protonated -OH₂⁺ at pH lower than 3,) as well as iron ions (Fe³⁺). These ions are known to interact with ligands, in particular with carboxylates.^{25,26} This kind of interaction is what we expect to occur when maghemite NPs are reacted with DCAA and DTCA. This assumption is supported by FTIR spectra, wherein Fe₂O₃@DTCA and Fe₂O₃@DCAA both show a peak around 1630 cm⁻¹ (Figure S7) corresponding to the vibration of the C = O bond of the carboxylate.^{25,26} This band, together with broad bands at around 2900 cm⁻¹ corre-

259 sponding to the C-H stretching of -CH₂- and -CH₃, accounts for the successful surface functionalization with both
 260 DCAA and DTCA. Additional peaks also appear at 1397 cm⁻¹, 1420 cm⁻¹, 1100 cm⁻¹ corresponding to C=S stretching
 261 vibration (Figure S6). Upon polymerization, a peak appears at around 1400 cm⁻¹ on both MIP and NIP magnetic NPs,
 262 which corresponds to C-N vibrations of acrylamide, along with another one at around 1100 cm⁻¹ characteristic of C-C
 263 elongations in polymer chains. Additionally, the vibration band at 1660 cm⁻¹ (C=O stretching) and at 2900 cm⁻¹ (C-H
 264 stretching) are more intense when magnetic nanoparticles are covered with MIP that contains a large number of C=O
 265 groups in poly-(acrylamide) units. All these peaks account for a successful polymerization.



266
 267 **Figure 2.** FTIR spectra of (A) bare Fe₂O₃, Fe₂O₃@DTCA and Fe₂O₃@DTCA@MIP and (B) bare Fe₂O₃, Fe₂O₃@DCAA and
 268 Fe₂O₃@DCAA@MIP nanoparticles.

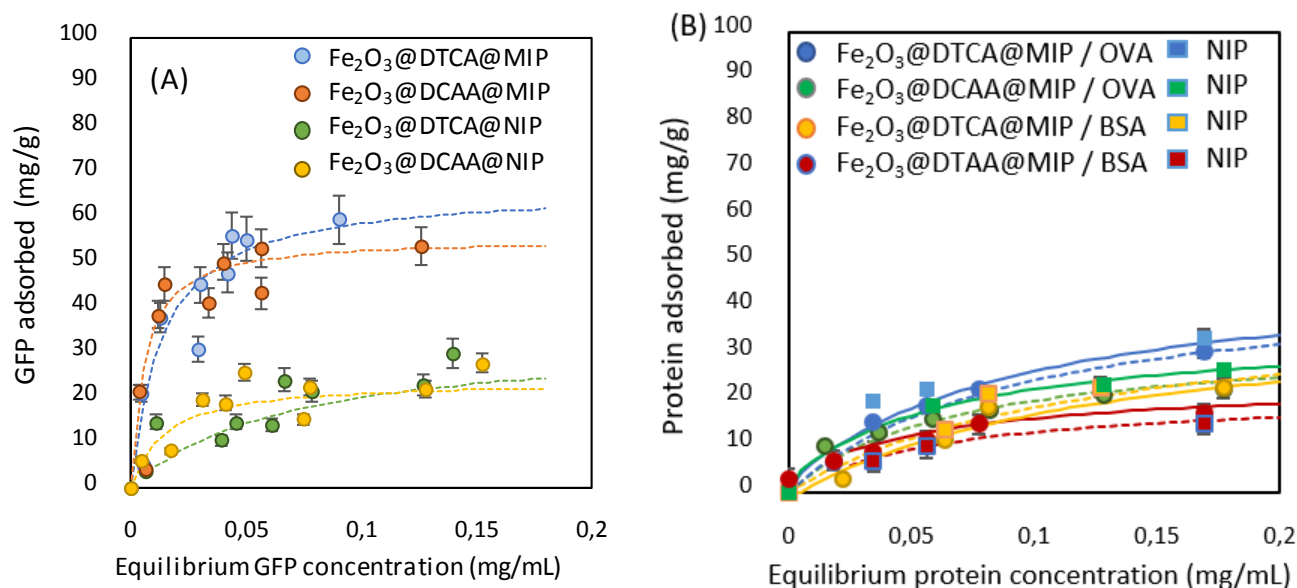


284 **Figure 3.** TGA of bare Fe₂O₃ (black), Fe₂O₃@DTCA (green) and Fe₂O₃@DTCA@MIP (green dashed line), Fe₂O₃@DCAA (blue) and
 285 Fe₂O₃@DCAA@MIP (blue dashed line) nanoparticles.

286
 287 To further characterize those nanocomposites, thermogravimetric analysis (TGA) was performed and thermograms are
 288 shown on Figure 3. DTCA and DCAA-functionalized SPIONs display weight losses of 15% and 11%, respectively. Such
 289 low value is due to the relatively low amount of the functionalizing agent. At the same time, weight losses corre-

290 sponding to organic compounds for MIP were 20% and 27 %, respectively, demonstrating the existence of a thin
 291 polymer layer.

292 In order to assess the ability of the nanocomposites to specifically and selectively recognize their target, isothermal
 293 adsorption experiments were performed by measuring the amount of adsorbed protein for various concentrations of
 294 GFP (from 0.01 to 2 mg/mL) incubated for 24 hours with a fixed concentration of nanocomposites (Figure 4). It is
 295 worthy to observe how MIPs bind much more GFP that corresponding NIPs; this relates to the absence of “binding
 296 sites” on NIPs, which, conversely to MIPs, results from the absence of the GFP template during their synthesis.



310 **Figure 4.** Adsorption isotherms of (A) Fe₂O₃@DCAA@MIP, Fe₂O₃@DCAA@NIP and Fe₂O₃@DTCA@MIP, Fe₂O₃@DTCA@NIP toward
 311 GFP and (B) MIP toward BSA and Ovalbumin. All experiments V = 3mL, 24h, fitted with a Langmuir adsorption model (Equation 1).

312 The adsorption equilibrium results on MIPs and on NIPs were found to fit the following linearized Langmuir isotherm:

$$\text{Equation (1): } \frac{C_e}{Q_e} = \frac{C_e}{Q_{max}} + \frac{1}{KQ_{max}}$$

314 where C_e is the equilibrium concentration of protein (mg/mL), Q_e is the equilibrium amount of adsorbed protein
 315 (mg/g), Q_{max} is the theoretical maximal amount of adsorbed protein (mg/g) and K is the association constant between
 316 protein and polymer matrix (mL/mg which can also be in L/mol). K_d and Q_{max} parameters were obtained by fitting the
 317 isotherms curves in Fig. 3 with the above-mentioned equation, and are recorded in Table 2. For each MIP, we
 318 calculated Q_{max} values higher than those of corresponding NIP, and really close to the experimental datum. The
 319 difference in GFP binding affinity to the MIP and NIP clearly indicate the role of the imprinting process in the
 320 formation of specific binding sites (Table 2). Correlation coefficient values R^2 of the fittings are high ($R^2 \geq 0.95$),
 321 suggesting that the Langmuir isotherm is an appropriate fitting for the equilibrium results.

Sample	Q_{max} (mg/g)	K_d (M ⁻¹)
Fe ₂ O ₃ @DCAA@MIP-GFP	55.6	5.2×10^5
Fe ₂ O ₃ @DCAA@MIP-OVA	23.0	
Fe ₂ O ₃ @DCAA@MIP-BSA	30.3	
Fe ₂ O ₃ @DCAA@NIP-GFP	25.6	8.1×10^4
Fe ₂ O ₃ @DCAA@NIP-OVA	27.4	
Fe ₂ O ₃ @DCAA@NIP-BSA	15.7	
Fe ₂ O ₃ @DTCA@MIP-GFP	66.7	6.1×10^5
Fe ₂ O ₃ @DTCA@MIP-OVA	18.3	

Fe ₂ O ₃ @DTCA@MIP-BSA	22.6	
Fe ₂ O ₃ @DTCA@NIP-GFP	34.4	2.8 10 ⁵
Fe ₂ O ₃ @DTCA@NIP-OVA	37.3	
Fe ₂ O ₃ @DTCA@NIP-BSA	24.5	

Table 2. Adsorption parameters for GFP, BSA, OVA on NIP and MIP.

We then also tested the selectivity of the magnetic materials towards two different proteins: ovalbumin (labelled OVA) and bovin serum albumin (labelled BSA). As shown in Figure 4B, the adsorption of BSA and OVA on Fe₂O₃@DCAA@MIP and Fe₂O₃@DTCA@MIP is much lower than that of GFP and are equivalent to the binding of Fe₂O₃@DCAA@NIP and Fe₂O₃@DTCA@NIP toward GFP, BSA and OVA. This shows that the binding sites on MIPs are selective and able to discriminate among different proteins and demonstrate the non-specific interactions of the proteins conversely to GFP. The Q_{max} values (Table 2) confirm this observation. In order to confirm the selectivity of Fe₂O₃@DCAA@MIP and Fe₂O₃@DTCA@MIP, we used OVA and BSA as competitive proteins. As displayed on Figure S9, Fe₂O₃@DCAA@MIP adsorb more GFP (41.2 and 38.5mg/g) than the other proteins (OVA: 18.6 and BSA: 20.2mg/g) when GFP and OVA or GFP and BSA are mixed together at the same concentration with the particles, even if one can notice the presence of some non-specific adsorption. The same behaviour was observed for Fe₂O₃@DTCA@MIP toward GFP (56.3mg/g and 48.3 mg/g) over the other proteins (OVA: 19.3mg/g and BSA: 21.2mg/g). Fe₂O₃@DCAA@MIP and Fe₂O₃@DTCA@MIP are thus able to specifically adsorb their template protein.

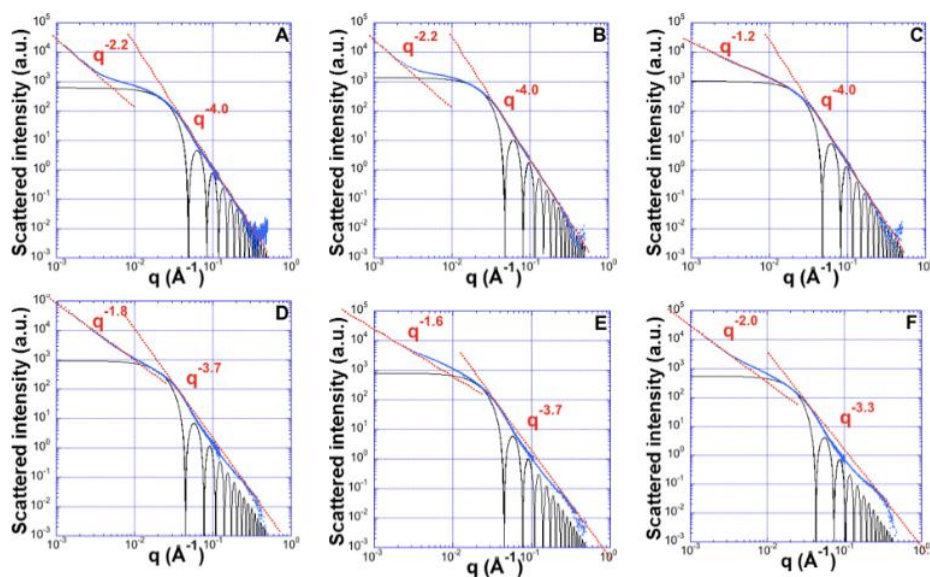
In a previous publication, we functionalized SPIONs with a low hydrophilic photoiniferter (diethyldithiocarbamate benzyldiazonium tetra-fluoroborate salt)²⁷ rather than DTCA or DCAA. As a result, DLS analyses on magnetic MIP indicated that the hydrodynamic diameter was 225nm, which is almost 4 times higher than what we obtained on Fe₂O₃@DCAA-MIP, and most importantly unsuited for *in vivo* applications. The adsorption results of GFP on such magnetic MIPs also showed a lower Q_{max} (47.4 mg/g). This may be due to the lower surface accessible to the proteins when the particles are bigger.

In order to gain more insights about the size and nanoparticles aggregation into the core of the synthesized composites before and after polymerization, and even after GFP adsorption at two different concentrations, we run SAXS experiments directly in aqueous media. In SAXS experiments, iron particles scatter the X-rays much more than the polymer layer, thus this analysis provides precious pieces of information concerning the magnetic cores.

The curves corresponding to γ -Fe₂O₃ NPs is presented in Figure 5A together with the theoretical form factor calculated for spheres with a radius of 9.2nm. The experimental curve exhibits a typical q⁻⁴ behavior at high q and follows the theoretical form factor. The fact that the oscillations are smeared out is linked to the polydispersity of the particles. Indeed, it is well known that even a low polydispersity "kills" the oscillations observed for perfectly monodisperse particles. Still, the results are perfectly coherent with the size determined by TEM (Table 1). At low q and therefore for large distances, the SAXS curve exhibits an upward deviation with a slope of -2.2, revealing the presence of aggregates in the suspensions with a fractal dimensions of 2.2, a classical value often observed for reaction limited aggregation processes²⁸. Upon surface modification with photoiniferters, the SAXS curves (Figure S10A, S6B) are almost identical to that obtained for bare nanoparticles, the only marginal difference being a possible slight increase in particle size with radii evolving from 9.2 to 9.4 nm. Surprisingly, the polymerization of a NIP layer does not significantly modify the SAXS curve (Figure S10C), whereas the polymerization of a MIP makes significant changes (Figure 5B and C).

Upon protein adsorption, further changes can be observed on the SAXS curves (Figure 5D, E, F). Indeed, at high q, a deviation from the q⁻⁴ behavior can be observed and the size corresponding to the best fit of the form factor increases to 10nm. Such a behavior could be associated to a rougher surface of the iron nanoparticles after protein adsorption. It

363 must be pointed out that such tendency is even more marked in the case of DTCA RAFT agent when more protein is
 364 adsorbed on the surface (Figure 5F). In addition, the slopes observed in the low q region are slightly higher than those
 365 measured before protein adsorption, which suggests a change in the aggregation mode. The use of SAXS then clearly
 366 allows obtaining information about the status of the various particles directly in aqueous media without any drying
 367 step typical of TEM analysis. Also, to the best of our knowledge, this is the first time SAXS that was used to compare
 368 the materials before and after protein adsorption.



385 **Figure 5.** SAXS results obtained for A = γ -Fe₂O₃, B = Fe₂O₃@DCAA@MIP, C = Fe₂O₃@DTCA@MIP, D =
 386 Fe₂O₃@DCAA@MIP-G, E = Fe₂O₃@DTCA@MIP-G and F = Fe₂O₃@DTCA@MIP-G+. G represents the adsorption of GFP
 387 on MIP at a concentration of 0,01mg/mL and G+ at a concentration of 0,1 mg/mL.

389 4. Conclusions

391 In conclusion, we have developed an easy and straightforward pathway to coat SPIONs with a thin layer imprinted
 392 against GFP as model protein, by photoiniferter mediated radical polymerization in aqueous media. This approach lies
 393 on the use of water soluble photoiniferters which simultaneously allow for NPs stabilization and polymer growth. The
 394 resulting superparamagnetic nano-MIPs featured sizes well below 100 nm, judged by DLS, TEM and SAXS analyses,
 395 and high adsorption capacity for GFP and selectivity over ovalbumin and bovine serum albumin. Moreover, the
 396 affinity constants measured on these nanocomposites were close to the biological ones, as previously obtained²⁹. As
 397 this synthetic approach has proved to be robust toward GFP, we strongly believe that it will also apply to a whole new
 398 range of other proteins, which could be helpful for biomedical as well as analytical applications.

400 **Funding:** "This research received no external funding"

401 **Conflicts of Interest:** "The authors declare no conflict of interest."

402 **Acknowledgement:** The authors are grateful to Aude Michel and Maylis Garnier for their help while characterizing the different
 403 nano-objects and the synthesis of the magnetic nanoparticles.

405 References

- 407 1. H. Zhang, *Adv. Mater.* 2019, **32**, 1806328.
- 408 2. F. Canfarotta, L. Lezina, A. Guerreiro, J. Czulak, A. Petukhov, A. Daks, K. Smolinska-Kempisty, A. Poma, S. Piletsky and
409 N.A. Barlev, *Nano Lett.* 2018, **18**, 4641.
- 410 3. A.E. Ekpenyong-Akiba, F. Canfarotta, B. Abd H., M Poblocka, M Casulleras, L Castilla-Vallmanya, G Kocsis-Fodor, M.E.
411 Kelly, J. Janus, M. Althubiti, E. Piletska, S. Piletsky and S. Macip, *Nanoscale Horiz.*, 2019, **4**, 757.
- 412 4. A. Cecchini, V. Raffa, F. Canfarotta, G. Signore, S. Piletsky, M.P. MacDonald and A. Cuschieri, *Nano Lett.* 2017, **17**, 2307.
- 413 5. H. Koide, K. Yoshimatsu, Y. Hoshino, S.H. Lee, A. Okajima, S. Ariizumi, Y. Narita, Y. Yonamine, A.C. Weisman, Y.
414 Nishimura, N. Oku, Y. Miura and K.J. Shea, *Nat. Chem.*, 2017, **9**, 715.
- 415 6. E. Verheyen, J.P. Schillemans, M. van Wijk, M.A. Demeniex, W.E. Hennink and C.F. van Nostrum, *Biomaterials*, 2011, **32**,
416 3008.
- 417 7. Y. Bao, J.A. Sherwood and Z. Sun, *J. Mater. Chem. C*, 2018, **6**, 1280.
- 418 8. S. Palanisamyab and Y.M. Wang *Dalton Trans.*, 2019, **48**, 9490.
- 419 9. M.D. Norris, K. Seidel, A. Kirschning, *Adv. Therap.*, 2019, **2**, 18000922019.
- 420 10. R.A. Revia, M. Zhang, *Materialstoday*, 2016, **19**, 157.
- 421 11. N. Griffete, J. Fresnais, A. Espinosa, C. Wilhelm, A. Bée and C. Ménager *Nanoscale*, 2015, **7**, 18891.
- 422 12. E. Cazares, M. Nerantzaki, J. Fresnais, C. Wilhelm, N. Griffete and C. Ménager *Nanomaterials*, 2018, **8**, 850.
- 423 13. M. Nerantzaki, A. Michel, E. Briot, J.M. Siaugue, C. Ménager, C. Wilhelm and N. Griffete *Chem. Comm.*, 2020, **56**, 10255.
- 424 14. E. Asadi, M. Abdouss, R.M. Leblanc, N. Ezzati, J. N. Wilson, *RSC Adv.* **2016**, 6 (43), 37308.
- 425 15. W. Li, M. Chen, H. Xiong, W. Wen, H. He, X. Zhang and W. Shengfu, *New J. Chem.*, 2016, **40**, 564.
- 426 16. C. Boitard, A.L. Rollet, C. Ménager and N. Griffete, *Chem. Comm.*, 2017, **53**, 8846.
- 427 17. Y. He, S. Tan, A.M.Abd El-A.A. Hacmüftüoğlud and Y. She, *RSC Adv.*, 2019, **9**, 29998.
- 428 18. C. Gonzato, M. Courty, P. Pasetto and K. Haupt, *Adv. Funct. Mat.*, 2011, **21**, 3947.
- 429 19. S. Beyazit, B.T.S. Bui, K. Haupt, C. Gonzato, *Progress in Polymer Science*, 2016, **62**, 1.
- 430 20. T. Otsu, *J. Polym. Sci. A Polym. Chem.*, 2000, **38**, 2121.
- 431 21. K. Ishizu, R.A. Khan, Y. Ohta, M. Furo, *Acid. J. Polym. Sci. A Polym. Chem.*, 2003, **42**, 76.
- 432 22. H. Sunayama, T. Ooya, T. Takeuchi, *Biosens. Bioelectron.*, 2010, **26**, 458.
- 433 23. J. Xu, K. Haupt, B. Tse Sum Bui, *ACS Appl. Mater. Interfaces*, 2017, **9**, 24476.
- 434 24. N. Hoshyar, S. Gray, H. Han, G. Bao *Nanomedicine*, 2016, **11**, 673.
- 435 25. M. A. G. Soler, G. B. Alcantara, F. Q. Soares, W. R. Viali, P. P. C. Sartoratto, J. R. L. Fernandez, S. W. da Silva, V. K. Garg, A.
436 C. Oliveira, P.C. Morais, *ECOSS-24*, 2007, **601**, 3921.
- 437 26. S. Yu, G. M. Chow, *J. Mater. Chem.*, 2004, **14**, 2781.
- 438 27. C. Boitard, A. Lamouri, C. Ménager, N. Griffete *ACS Applied Polymer Materials*, 2019, **1**, 928.
- 439 28. R. Jullien, M. Kolb, *J. Phys. A: Math. Gen.*, 1984, **17**, L639
- 440 29. Z. Zhang, Y. Wang, Y. Ding, M. Hattori *Scientific Reports*, 2020, **10**, 1.
- 441
- 442
- 443
- 444
- 445
- 446
- 447
- 448

449

450